Percolative properties of hard oblate ellipsoids of revolution with a soft shell

Gianluca Ambrosetti,[1,2,*] Niklaus Johner,[1] Claudio Grimaldi,[1] Andrea Danani,[2] and Peter Ryser[1]
[1]*LPM, Ecole Polytechnique Fédérale de Lausanne, Station 17, CH-1015 Lausanne, Switzerland*
[2]*ICIMSI, University of Applied Sciences of Southern Switzerland, CH-6928 Manno, Switzerland*
(Received 8 May 2008; revised manuscript received 31 July 2008; published 23 December 2008)

We present an in-depth analysis of the geometrical percolation behavior in the continuum of random assemblies of hard oblate ellipsoids of revolution. Simulations were carried out by considering a broad range of aspect ratios, from spheres up to aspect-ratio-100 platelike objects, and with various limiting two-particle interaction distances, from 0.05 times the major axis up to 4.0 times the major axis. We confirm the widely reported trend of a consistent lowering of the hard particle critical volume fraction with increase of the aspect ratio. Moreover, by assimilating the limiting interaction distance to a shell of constant thickness surrounding the ellipsoids, we propose a simple relation based on the total excluded volume of these objects which allows us to estimate the critical concentration from a quantity that is quasi-invariant over a large spectrum of limiting interaction distances. Excluded volume and volume quantities are derived explicitly.

DOI: 10.1103/PhysRevE.78.061126 PACS number(s): 64.60.ah, 72.80.Tm, 05.70.Fh

I. INTRODUCTION

A central problem in materials science is the precise evaluation of the percolation threshold of random particle dispersions embedded in a continuous medium. This occurs typically in composite materials and is of importance for the prediction of relevant properties such as the electrical conduction in insulator-conductor composites. Practical examples include carbonaceous fillers like carbon fibers, graphite, carbon black, carbon nanotubes, and fullerenes, but also metallic and ceramic ones, while matrices can be, for instance, polymeric, metallic, or ceramic. Although the most studied particle form is the sphere (see, e.g., [1–6]), a broad range of fillers in real composites have forms which deviate consistently from the sphere. Previous investigations have considered different particle shapes like, e.g., sticks [7–11], wavy sticks [12], plates [13–15], or ellipsoids [16–20], in the fully penetrable case, where the particles are allowed to freely overlap. Only a few works have dealt with nonspherical hard objects surrounded with a soft shell, like hard sticks [4,21–23] or triaxial polydisperse ellipsoids [24], while a recent paper [25] contemplated, as in the present study, the case of hard ellipsoids of revolution, but in the prolate domain.

The widespread use of composites containing fibrous fillers has made the stick, or other elongated object, the favorite nonspherical shape in many studies. Nevertheless, some other fillers, notably graphite, have shapes that are better assimilable to flattened ellipsoids or platelets, and over a broad range of aspect ratios, i.e., ratios of longer to shorter dimension. Therefore, the exploration of the relatively uncharted terrain of the percolative properties of oblate objects as a function of their aspect ratio is the aim of the present study.

In this paper we consider the special case of oblate *ellipsoids of revolution*, usually called (oblate) *spheroids*, which are ellipsoids with two equal (major) axes and may be obtained by rotation of a two-dimensional (2D) ellipse around its minor axis. The reasons for this choice are twofold: first, spheroids are characterized by a smaller number of parameters (seven, against nine of the general ellipsoid); second, experimental measurement techniques of the filler particle size distributions are generally able to extract only major and minor dimensions, making it difficult to quantitatively define a size distribution for the third axis.

Our model is defined by a dispersion of impenetrable spheroids of identical dimensions with isotropic distribution of the symmetry axis orientation. Given any two spheroids, a connectivity criterion is introduced by allowing an upper cutoff distance beyond which the two spheroids are considered disconnected. More precisely, each spheroid is coated with a penetrable shell of constant thickness, and two particles are connected if their shells overlap. In a system of conducting spheroids dispersed in an insulating continuum host, the shell thickness can be physically interpreted as a typical tunneling length between the particles, governing the electrical connectivity of the composite. Note that the inclusion of a constant thickness shell leads to a shape of the total object which is no longer that of a spheroid. On the other side, a penetrable shell consisting of an enlarged spheroid, as studied in [25] for the case of prolate ellipsoids, implies increasingly nonuniform shell thicknesses as the aspect ratio gets higher.

To carry out our investigation we exploit a simulation algorithm, described in the following section, that allows us to determine the percolation behavior of a random distribution of impenetrable spheroids as a function of their volume fraction, aspect ratio, shell thickness, and simulation cell size.

II. THE SIMULATION ALGORITHM

To build an algorithm which allows us to numerically investigate the percolative properties of the proposed system, we first need a routine that generates a random distribution of nonoverlapping ellipsoids (spheroids) and that calculates their interdistance (meant as the minimal distance between two ellipsoid surfaces). For this purpose we may require two

*gianluca.ambrosetti@epfl.ch

functions, an ellipsoid overlap criterion and the distance between two ellipsoids, the first being needed of course only if it can be computed in a time consistently shorter than the second. Neither of these functions allows simple closed form solutions, but some evaluation techniques are nevertheless available [17,18,26–28]. We have chosen the approach proposed by Rimon and Boyd (RB) [29,30] which was used for an obstacle collision detection procedure for robots, where short computational times are essential. The RB technique allows two key benefits: (1) A quick estimation procedure of the distance between two ellipsoids that uses standard computation routines and that can be made sufficiently precise; (2) an overlap criterion between two ellipsoids as an intermediate result for the interdistance computation, which can be calculated in about half the time needed for the complete calculation. The computation is based on a formula for the distance of a point from an ellipsoid which reduces the problem to the calculation of the minimal eigenvalue of an auxiliary matrix constructed from the geometrical data. Details are given in Appendix A.

We are now going to briefly outline how the distribution generation algorithm is constructed. First, a spheroid distribution is created inside a cubic cell of volume L^3 by random sequential addition: for every new particle, random placing is attempted and accepted as valid only if there is no overlap with any neighboring particle. The spheroid angles are generated so as to assure an isotropic distribution of orientations [7,17]. To speed up the search for neighbors the main cubic cell is subdivided into discrete binning cells of size comparable to the major dimension of the spheroids. When checking for overlap, simple geometrical rejection criteria which can identify an inevitable overlap are used as a filter to avoid unnecessary computations of the (time-consuming) RB overlap function. Geometrical criteria to identify neighbors that are distant enough as not to be able to lead to an overlap in any case are also used, again to avoid unnecessary computations of the RB function. Periodic boundary conditions are imposed on the main cell. Second, the interparticle distance is computed. An interaction interdistance (equivalent to twice the penetrable shell thickness) is chosen so that spheroids separated by a distance greater than this are considered as noninteracting. Again, the same neighbor search procedure is used and, if necessary, the distance computation is performed. To do this in an efficient way, a first RB calculation is executed. If the resulting distance estimate is clearly beyond the interaction range (even when the worst possible error is considered) the calculation is stopped. Otherwise, the computation is continued by performing the RB calculation with inverted spheroids, comparing the outcome with the first calculation, and retaining the shorter of the two. Finally, a part of the RB computation is reiterated to obtain a further correction. When the results are compared with those of a more accurate but much slower distance evaluation routine, this procedure leads to a distance estimate that has an average error of about +1% on a wide range of ratios of distance to major spheroid dimension (from 10^{-4} to 10). Figure 1 shows one of such distributions as it appears when the algorithm output file is loaded in a viewer.

Once the desired distribution has been created and the neighboring-particle interdistances computed, the distribution algorithm output data are fed into the part of a program which isolates the connected cluster using a modified version of the Hoshen-Kopelman algorithm [31–33]. Finally, it is verified whether the connected cluster spans two specific opposite sides of the simulation cell.

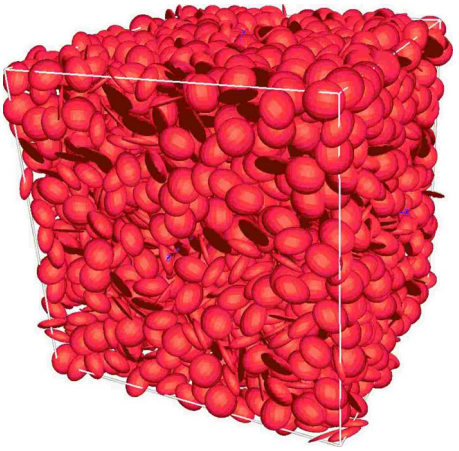

FIG. 1. (Color online) Distribution of 3000 spheroids with aspect ratio $a/b=10$.

III. SIMULATION RESULTS

To explore the percolative properties of hard oblate spheroids surrounded with a penetrable shell of constant thickness, we considered spheroids with an aspect ratio, i.e., ratio of spheroid major axis a to minor (symmetry) axis b, a/b, between 1 (spheres) and 100. The ratio of shell thickness d to spheroid major axis, d/a, was chosen to vary between 0.05 and 4.0. The thinnest shell limit is bound to the maximum volume fraction which can be achieved through random sequential addition [34] for the $a/b=1$ (spheres) case. Close to this limit, computation times grow enormously since it becomes increasingly difficult to find available space to place new particles [34]. For the lowest investigated shell thickness each aspect-ratio case needed several weeks of computing time on a modern dual-core machine.

To extrapolate the percolation threshold from the simulation algorithm, we followed finite-size scaling arguments as described in Ref. [35] and briefly outlined below. For a given size L of the cube, we obtained the spanning probability as a function of the spheroid volume fraction by recording the number of times a percolating cluster appeared over a given number of realizations. The resulting spanning probabilities were then plotted against the volume fraction and fitted with the sigmoidal function

$$f=\frac{1}{2}\left[1+\tanh\left(\frac{\phi-\phi_c^{\mathrm{eff}}}{\Delta}\right)\right], \tag{1}$$

where ϕ_c^{eff} is the percolation threshold for a given value of L and corresponds to the hard-particle volume fraction at which the spanning probability is equal to $1/2$, while Δ represents the width of the percolation transition. Both ϕ_c^{eff} and Δ depend on the size L of the system and, by following the scaling arguments of [35], allow us to deduce the percolation

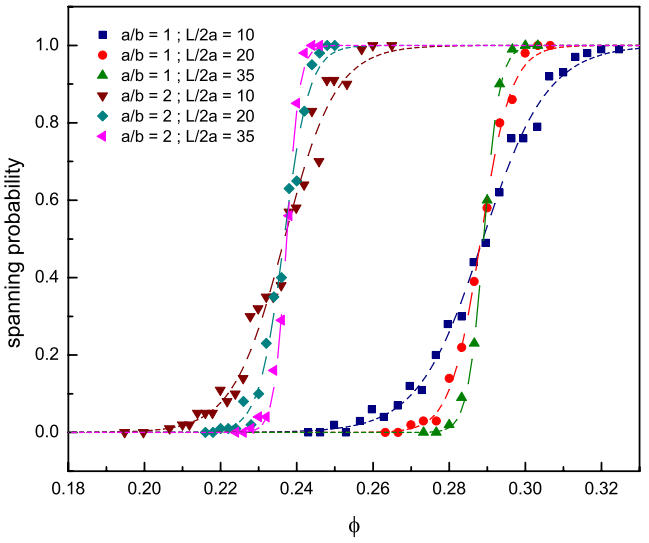

FIG. 2. (Color online) Percolation width variation with the increase of the simulation cell size for the aspect ratios 1 and 2. $d/a=0.1111$.

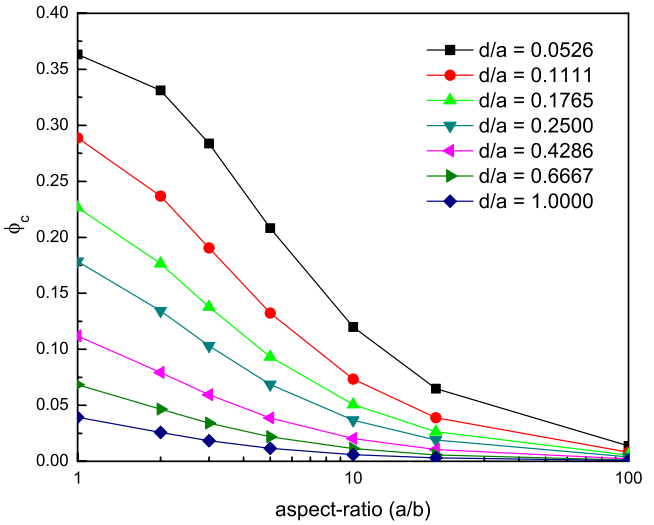

FIG. 3. (Color online) Percolation threshold ϕ_c variation as a function of the aspect ratio for different shell thicknesses.

threshold ϕ_c for the infinite system through the following scaling relations:

$$\Delta(L) \propto L^{-1/\nu}, \tag{2}$$

$$\phi_c^{\mathrm{eff}}(L) - \phi_c \propto L^{-1/\nu}, \tag{3}$$

where ν is the correlation length exponent. By repeating the simulation procedure for different cell sizes it is possible, via the percolation transition widths Δ and the inversion of Eq. (2), to extract ν and consequently, from Eq. (3), the percolation threshold ϕ_c for $L=\infty$. We choose to simulate ten different cell sizes, $L=10$, 13, 15, 17, 20, 23, 25, 27, 30, and 35 times the major spheroid dimension, i.e., twice the major axis a. For thick shells ($d/a \geqslant 1.0$) the cell sizes were increased further. The spheroid number was on the order of thousands for the smallest cells up to about 70 000 for the largest. The number of realizations per volume fraction step varied from 50 for the smallest shell thickness up to 400 for the thicker ones. Higher realization numbers did not show appreciable improvements [36]. In all cases, the correlation length exponent ν had a value around 0.9, in good agreement with previous results on spheres [2,31,35]. However, sometimes the fluctuations of ϕ_c^{eff} were too large and a simple average of the results provided a more significant result than the one obtained from the finite-size analysis.

In Fig. 2 we report the obtained spanning probability as a function of ϕ for $a/b=1$ and $a/b=2$ and for selected values of the cell size L. The shell thickness d to major axis ratio was set equal to $d/a=0.1111$. From the figure it is clear that increase in the aspect ratio from $a/b=1$ (spheres) to 2 leads to a lowering of the percolating volume fraction. This trend is confirmed in Fig. 3, where the critical hard-particle volume fraction ϕ_c is plotted as a function of a/b and for several values of the penetrable shell thickness. For the thinnest shells we find that ϕ_c can be reduced by about one order of magnitude in going from $a/b=1$ up to $a/b=100$. This result is fully consistent with the frequently reported trend that assemblies of oblate objects with high aspect ratios entail a lower percolation threshold. For example, several studies of graphite-polymer composites reported a consistent lowering of the electrical conductivity percolation threshold when very high-aspect-ratio graphite nanosheets [13,37,38] or graphene flakes [39] were used. We also note that for the $a/b=1$ (spheres) case there is full agreement between our ϕ_c and those of the literature [1,2,31].

In addition to ϕ_c, another quantity characterizing the percolation threshold is the reduced critical density η_c defined as

$$\eta_c = \rho_c V_d = \phi_c \frac{V_d}{V}, \tag{4}$$

where ρ_c is the number density at percolation and V_d is the total object volume, comprising the volume of the hard spheroid, V, plus that of the penetrable shell. V_d is explicitly calculated in Appendix B; see Eq. (B25). The behavior of η_c, plotted in Fig. 4 as a function of the penetrable shell thickness d/a and for several aspect ratios, accounts for the dependence of the percolation threshold on the geometry of the total object (hard core plus penetrable shell). Indeed, for $d/a=4$ the reduced critical density is almost independent of the aspect ratio a/b while, for thinner penetrable shells, η_c acquires a stronger dependence on a/b. This is due to the fact that, for large d/a values, the form of the total object does not deviate much from that of a sphere, so that $\eta_c \simeq 0.34$ as for fully penetrable spheres. On the contrary, for smaller values of d/a, the geometry of the total object is more similar to that of an oblate ellipsoid, with a consequently stronger dependence of η_c on the aspect ratio.

IV. QUASI-INVARIANTS AT THE PERCOLATION THRESHOLD

In continuum percolation, an important quantity providing information on the local topology of the percolating cluster is

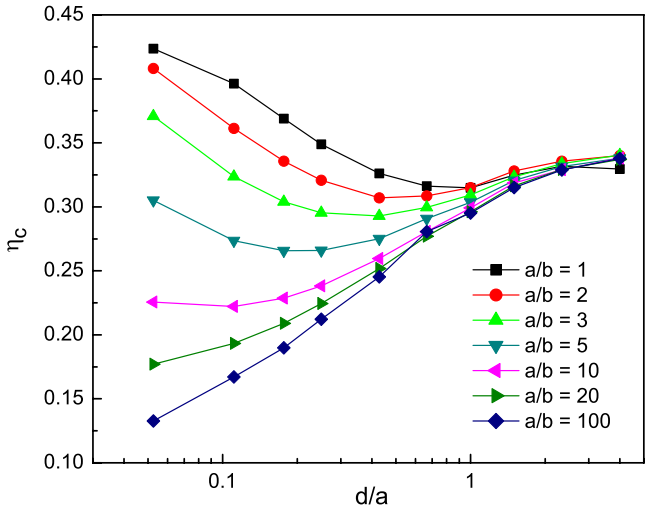

FIG. 4. (Color online) η_c as a function of the shell thickness for different aspect ratios.

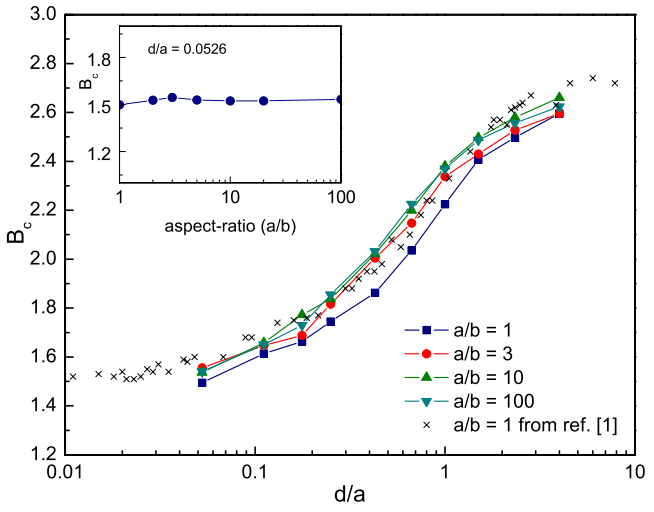

FIG. 5. (Color online) B_c as a function of the shell thickness from simulation for different aspect ratios. The results are obtained from the simulations by counting the connection number of each spheroid with its neighbors and averaging.

the average number B_c of objects connected to a given particle. For fully penetrable objects, and since in this case there is no spatial correlation, B_c is simply given by [10]

$$B_c = \rho_c V_{\mathrm{ex}}, \tag{5}$$

where V_{ex} is the excluded volume defined by the volume around an object where the center of another object cannot penetrate if overlap is to be avoided. For penetrable spheres each of volume V, the excluded volume is $V_{\mathrm{ex}}=8V$ and, by using $\rho_c=\eta_c/V$ with $\eta_c\simeq 0.34$, the resulting connectivity number is $B_c\simeq 2.74$, which agrees well with the evaluation of B_c from a direct enumeration of connections in assemblies of penetrable spheres at percolation [1,4]. Indeed, for fully penetrable spheres, for which the sphere centers are distributed randomly, Eq. (5) simply states that B_c is equivalent to the average number of centers found within an excluded volume, irrespective of the spatial configuration of the percolating objects. However, for semipenetrable spheres, the presence of a hard core introduces a spatial correlation (see below) so that B_c is expected to deviate from the uncorrelated case of Eq. (5). In particular, B_c is found to decrease as the hard-core portion of the sphere increases, reaching $B_c \simeq 1.5$ for very thin penetrable shells [1,4], as a result of the repulsion of the impenetrable hard cores.

Let us now consider the case of assemblies of oblate ellipsoids. In Fig. 5 we plot the computed values of B_c as a function of the penetrable shell thickness d/a and for selected values of the aspect ratio a/b. Results of Ref. [1], which extend to shell thicknesses below $d/a\simeq 0.05$ because of a different distribution generation procedure than random sequential addition, are also plotted for comparison. For $a/b=1$ we recover the results for the spheres: $B_c\simeq 2.7$ for large values of d/a while $B_c\simeq 1.5$ for $d/a=0.0526$. For $a/b>1$ and thick penetrable shells, B_c remains close to the spherical case also for larger aspect ratios because, as said before, for large d/a values the entire object (hard core plus penetrable shell) is basically a semipenetrable sphere with a small hard-core spheroid. However, by decreasing d/a, we find that B_c continues to remain very close to the $a/b=1$ case also for the thinnest penetrable shells, irrespective of the aspect ratio. This is well illustrated by the inset of Fig. 5, where the calculated B_c for $d/a=0.0526$ does not show appreciable variations over a two-order-of-magnitude change of a/b. This result is rather interesting in view of the fact that the quasi-invariance of B_c with respect to the aspect ratio in oblate spheroids is in striking contrast to what is found by numerical evaluation for prolate hard objects such as spherocylinders [4,21]. For example, for spherocylinders made of hard cylinders of length H and diameter D capped by hemispheres and with penetrable shells of thickness $0.1D$, B_c is found to decrease from $B_c=1.61$ for $H/D=4$ down to $B_c=1.29$ at $H/D=25$ [21], consistently deviating therefore from $B_c\simeq 1.76$, obtained for spheres of diameter D and the same penetrable shell thickness [1]. Different behaviors of quasi-impenetrable oblate and prolate objects noted here are also found in the fully penetrable case. Indeed, B_c of prolate objects decreases as the aspect ratio is increased, and is expected to approach unity in the extreme prolate limit as a consequence of the vanishing critical density [8], while B_c of oblate objects remains close to $B_c\simeq 3$ all the way from the moderate to the extreme oblate regimes [18].

Now we can write a general relation between the average connection number B_c at percolation and the critical number density ρ_c. If we consider hard spheroids with penetrable shell and with an isotropic distribution of orientations, then B_c reduces to

$$B_c = \rho_c \int_0^{2\pi} d\theta \int_0^{\pi} d\varphi\, \Phi(\theta,\varphi) \int_{V_{\mathrm{excl}}(\theta,\varphi)} d^3\mathbf{r}\, g(\mathbf{r},\theta,\varphi), \tag{6}$$

where θ and φ are the angles between the major axes of two spheroids separated by $\mathbf{r}$ and $g(\mathbf{r},\theta,\varphi)$ is the radial distribution function: given a particle centered in the origin, $\rho_c g(\mathbf{r},\theta,\varphi)$ represents the mean particle number density at position $\mathbf{r}$ with a orientation θ,φ. The integration over $\mathbf{r}$ is

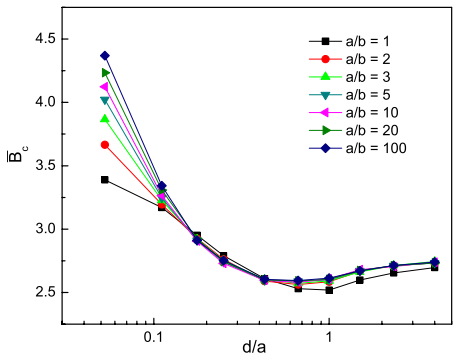

FIG. 6. (Color online) $\bar{B}_c$ as a function of the shell thickness for different aspect ratios.

performed over the total excluded volume $V_{\mathrm{exd}}(\theta,\varphi)$ (hard core plus penetrable shell) centered at the origin and having orientation θ,φ.

We observe that all the information about the presence of a hard core inside the particles is included in the radial distribution function, which will be zero in the volume occupied by the hard core of the particle centered at the origin. However, $g(\mathbf{r},\theta,\varphi)$ is a rather complex function and even for the case of spheres there are only approximate theoretical expressions [40]. Also, the construction of a fitted expression to simulation data may turn out to be excessively complicated when the respective orientation of the particles has to be taken into account.

The lowest-order approximation that we may then consider, and which is exact in the case of fully penetrable particles, is the one where $g(\mathbf{r},\theta,\varphi)=1$. This is equivalent to neglecting all contributions of the radial distribution function which come from the presence of the hard core. The resulting quantity, which we denote by $\bar{B}_c$, is then given by

$$\bar{B}_c = \rho_c \int_0^{2\pi} d\theta \int_0^{\pi} d\varphi\, \Phi(\theta,\varphi) \int_{V_{\mathrm{exd}}(\theta,\varphi)} d\mathbf{r} = \rho_c \langle V_{\mathrm{exd}} \rangle, \quad (7)$$

where $\langle V_{\mathrm{exd}} \rangle$ is the orientation-averaged total excluded volume. Given the averaged excluded volume of spheroids surrounded with a shell of constant thickness $\langle V_{\mathrm{exd}} \rangle$ (B29), together with the hard spheroid excluded volume expression (B28) or (B30), we can calculate $\bar{B}_c$ from the percolation threshold results obtained from the simulations:

$$\bar{B}_c = \rho_c \langle V_{\mathrm{exd}} \rangle = \phi_c \frac{\langle V_{\mathrm{exd}} \rangle}{V}, \quad (8)$$

where we have used the hard-core volume fraction ϕ_c. The full details of the calculation of the excluded volume quantities can be found in Appendix B. The resulting values of $\bar{B}_c$ are plotted in Fig. 6 as a function of the penetrable shell thickness and for several aspect ratios. $\bar{B}_c$, which can be interpreted as the average number of particle centers per averaged excluded volume, is a different quantity from B_c and a correspondence between the two appears only in the thick shell limit, where the system is more similar to a fully penetrable one. This can be appreciated by comparing Fig. 6 with Fig. 5. The increasing discrepancy for thinner shells is due to stronger correlation effects stemming from the presence of the hard core. Nevertheless, the behavior of $\bar{B}_c$ is still rather intriguing. Indeed, the dependence of $\bar{B}_c$ on the penetrable shell thickness d/a appears to be universal with respect to the aspect ratio, for all d/a values larger than $d/a > 0.1$. Furthermore, in this region of d/a, $\bar{B}_c$ has a rather weak dependence on the shell thickness, not deviating much from $\bar{B}_c \simeq 2.8$.

The quasi-invariance of $\bar{B}_c$ may be a result of practical utility since, by using Eq. (8), the percolation threshold ϕ_c can be estimated from $\langle V_{\mathrm{exd}} \rangle$ and $\bar{B}_c \simeq 2.8$, in a wide interval of d/a and aspect-ratio values. The direct determination of the percolation threshold of hard oblate spheroids via simulations is a time-consuming procedure. Thus, a relation which allows us to quickly evaluate such a quantity as a function of the dispersion geometric parameters offers some advantage.

V. CONCLUSIONS

The geometrical percolation threshold in the continuum of random distributions of oblate hard ellipsoids of revolution surrounded with a soft shell of constant thickness has been investigated. Simulation results spanning a broad range of aspect ratios (from $a/b=1$ to 100) and shell thickness (from $d/a \simeq 0.05$ to $d/a=4$) values have been reported. It is found that larger aspect ratios entail lower percolation thresholds, in agreement with the behavior observed experimentally in insulator-conductor composites where the conducting phase is constituted by oblate objects, such as graphite nanosheets. For the thinnest investigated shell ($d/a \simeq 0.05$), the percolation threshold of the aspect-ratio-100 platelike objects was more than 26 times lower than the one of spheres. Furthermore, the average number B_c of connected objects at percolation is a quasi-invariant with respect to the aspect ratio, in contrast with what has been previously reported for prolate objects. Indeed, for all the considered aspect ratios a behavior of B_c was found that is almost identical to that obtained for spheres. Finally, we have identified an additional quasi-invariant of the investigated system, $\bar{B}_c$, which is based on the excluded volume concept and which allows us to quickly infer the system percolation threshold. For all penetrable shells thicker than $d/a=0.1$, $\bar{B}_c$ shows almost no aspect-ratio dependence and remains close to $\bar{B}_c \simeq 2.8$.

ACKNOWLEDGMENTS

This study was supported by the Swiss Commission for Technological Innovation (CTI) through project GraPoly, (CTI Grant No. 8597.2), a joint collaboration led by TIMCAL Graphite & Carbon SA. Simulations were performed at the ICIMSI facilities with the help of Eric Jaminet. Data analysis was carried out with the help of Ermanno Oberrauch. Comments by I. Balberg were greatly appreciated.

APPENDIX A: GENERALIZED DISTANCE BETWEEN ELLIPSOIDS AND OVERLAP CRITERION

We outline in this appendix the mathematical details of the ellipsoid interdistance evaluation procedure and overlap criterion as introduced by Rimon and Boyd [29,30]. Given two ellipsoids ε_A and ε_B identified by their 3×3 form matrices $\hat{A}$ and $\hat{B}$ and centered at $\mathbf{c}_A$ and $\mathbf{c}_B$, respectively,

$$(\mathbf{x}-\mathbf{c}_A)^T\hat{A}(\mathbf{x}-\mathbf{c}_A)=0, \quad \varepsilon_A, \tag{A1}$$

$$(\mathbf{x}-\mathbf{c}_B)^T\hat{B}(\mathbf{x}-\mathbf{c}_B)=0, \quad \varepsilon_B, \tag{A2}$$

we have that the minimal distance d between the ellipsoids can be estimated as

$$d(\varepsilon_A,\varepsilon_B)=\|\mathbf{x}^*-\mathbf{y}^*\|, \tag{A3}$$

where

$$\mathbf{x}^*=\mathbf{c}_A+\lambda\hat{A}^{-1/2}[\lambda\mathbf{I}_{3\times3}-(\hat{A}^{-1/2}\hat{B}\hat{A}^{-1/2})^{-1}]^{-1}\hat{A}^{1/2}(\mathbf{c}_B-\mathbf{c}_A) \tag{A4}$$

and λ is the minimal eigenvalue of the 6×6 matrix

$$\begin{pmatrix} (\hat{A}^{-1/2}\hat{B}\hat{A}^{-1/2})^{-1} & -\mathbf{I}_{3\times3} \\ -[(\hat{A}^{-1/2}\hat{B}\hat{A}^{-1/2})^{-1/2}\hat{A}^{1/2}(\mathbf{c}_B-\mathbf{c}_A)][(\hat{A}^{-1/2}\hat{B}\hat{A}^{-1/2})^{-1/2}\hat{A}^{1/2}(\mathbf{c}_B-\mathbf{c}_A)]^T & (\hat{A}^{-1/2}\hat{B}\hat{A}^{-1/2})^{-1} \end{pmatrix}, \tag{A5}$$

while

$$\mathbf{y}^*=\mathbf{x}^*+\mu(\mu\mathbf{I}_{3x3}-\hat{A}^{-1})(\mathbf{c}_A-\mathbf{x}^*) \tag{A6}$$

and μ is the minimal eigenvalue of the 6×6 matrix,

$$\begin{pmatrix} \hat{A}^{-1} & -\mathbf{I}_{3\times3} \\ -[\hat{A}^{-1/2}(\mathbf{c}_A-\mathbf{x}^*)][\hat{A}^{-1/2}(\mathbf{c}_A-\mathbf{x}^*)]^T & \hat{A}^{-1} \end{pmatrix}. \tag{A7}$$

$\mathbf{I}_{3\times3}$ is naturally the 3×3 identity matrix.

The overlap criterion comes from $\mathbf{x}^*$ alone. If we construct the quantity

$$m(\varepsilon_A,\varepsilon_B)\equiv(\mathbf{x}^*-\mathbf{c}_A)^T\hat{A}(\mathbf{x}^*-\mathbf{c}_A)-1, \tag{A8}$$

we will have that

$$\begin{aligned} m<0, &\quad \varepsilon_A,\varepsilon_B \text{ overlap}, \\ m=0, &\quad \varepsilon_A,\varepsilon_B \text{ touch}, \\ m>0 &\quad \text{otherwise}. \end{aligned} \tag{A9}$$

The algorithm implementation followed then the route outlined by RB [29,30] although in the present case we have used FORTRAN 90 instead of C as programming language.

APPENDIX B: EVALUATION OF EXCLUDED VOLUME QUANTITIES

We report in the following the derivation of the excluded volume of two oblate spheroids, the excluded volume of two oblate spheroids surrounded with a shell of constant thickness, and their angular averages. We follow a route due to the pioneering work of Isihara [41] which is somewhat more laborious than the one used by the same author [42] and the authors of [43] to derive the widely used Isihara-Ogston-Winzor spheroid excluded volume formula. The advantage is that it is possible to obtain, albeit in a series expansion form, the excluded quantities with their full angle dependence. The average over the spheroid angle distribution function is performed successively and can be easily extended to nonisotropic cases. Let us consider the case of two identical spheroids of major axis a and minor axis b in contact, as illustrated in Fig. 7.

The geometrical quantities H and K, which represent the distances from the spheroid centers to the tangent plane to the two spheroids in the contact point, may be written as

$$H(\alpha)=a\sqrt{1-\epsilon^2\cos^2\alpha}, \tag{B1}$$

$$K(\alpha')=a\sqrt{1-\epsilon^2\cos^2\alpha'}, \tag{B2}$$

where ϵ represents the *eccentricity* (for oblate spheroids)

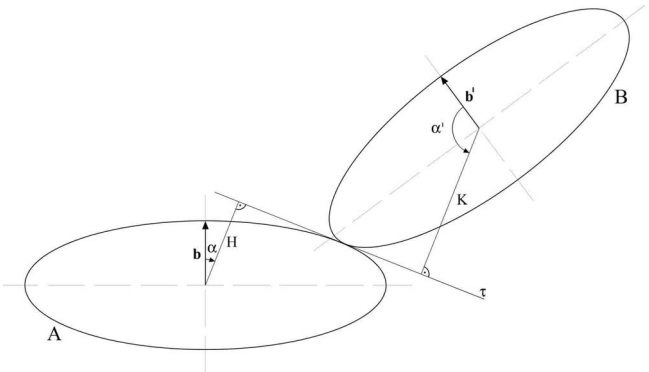

FIG. 7. Two identical oblate spheroids in contact (2D representation).

$$\epsilon \equiv \sqrt{1-\frac{b^2}{a^2}}. \tag{B3}$$

Furthermore, we have

$$\begin{aligned}\cos^2\alpha' &= [\sin\varphi\sin\alpha(\cos\theta\cos\beta+\sin\theta\sin\beta)\\ &\quad+\cos\varphi\cos\alpha]^2\\ &= [\sin\varphi\sin\alpha\cos(\beta-\theta)+\cos\varphi\cos\alpha]^2,\end{aligned} \tag{B4}$$

where θ and φ are the angles which define the rotation that transforms the symmetry axis vector $\mathbf{b}$ of spheroid A into that of $B,\mathbf{b}'$.

We can then write the excluded volume of two identical spheroids, or more generally two identical ovaloids, as [41,42]

$$V_{\mathrm{ex}} = 2V + \int K(H,H)d\omega = 2V + \int_0^{2\pi} d\beta \int_0^{\pi} d\alpha \sin\alpha K(H,H), \tag{B5}$$

where $d\omega$ is the infinitesimal surface element of the unit sphere centered at the origin which, by using the reference frame choice of Fig. 7, takes the form

$$d\omega = \sin\alpha\, d\alpha\, d\beta. \tag{B6}$$

Furthermore, in Eq. (B5) we have introduced the differential operator on the unit sphere which for two equal scalar quantities F takes the form

$$(F,F) \equiv 2\left\{\left(\frac{\partial^2 F}{\partial\alpha^2}+F\right)\left(\frac{1}{\sin^2\alpha}\frac{\partial^2 F}{\partial\beta^2}+\frac{\cos\alpha}{\sin\alpha}\frac{\partial F}{\partial\alpha}+F\right) - \left[\frac{\partial}{\partial\alpha}\left(\frac{1}{\sin\alpha}\frac{\partial F}{\partial\beta}\right)\right]^2\right\}, \tag{B7}$$

while V is the volume of the spheroid.

With the explicit form of H, Eq. (B1), K, Eq. (B2), and relation (B4), we can write for the excluded volume (B5) in the case of the two spheroids the integral form

$$\begin{aligned}V_{\mathrm{ex}}(\theta,\varphi) &= 2V + 2a^3(1-\epsilon^2)\int_0^{2\pi} d\beta \int_0^{\pi} d\alpha \sin\alpha \frac{\sqrt{1-\epsilon^2\cos^2\alpha'}}{(1-\epsilon^2\cos^2\alpha)^2}\\ &= 2V + 2a^3(1-\epsilon^2)\underbrace{\int_0^{2\pi} d\beta \int_0^{\pi} d\alpha \sin\alpha \frac{\sqrt{1-\epsilon^2(\sin\varphi\sin\alpha\cos\beta+\cos\varphi\cos\alpha)^2}}{(1-\epsilon^2\cos^2\alpha)^2}}_{I},\end{aligned} \tag{B8}$$

where we have used the fact that

$$\begin{aligned}&\int_0^{2\pi} d\beta\sqrt{1-\epsilon^2[\sin\varphi\sin\alpha\cos(\beta-\theta)+\cos\varphi\cos\alpha]^2}\\ &= \int_0^{2\pi} d\beta\sqrt{1-\epsilon^2(\sin\varphi\sin\alpha\cos\beta+\cos\varphi\cos\alpha)^2},\end{aligned} \tag{B9}$$

because of the 2π periodicity of the integrand, which means that V_{ex} is θ independent.

We now may expand the $1-\epsilon^2(\sin\varphi\sin\alpha\cos\beta+\cos\varphi\cos\alpha)^2$ square root:

$$\begin{aligned}&\sqrt{1-\epsilon^2(\sin\varphi\sin\alpha\cos\beta+\cos\varphi\cos\alpha)^2}\\ &= 1-\frac{1}{2\sqrt{\pi}}\sum_{k=1}^{\infty}\Gamma\left(k-\frac{1}{2}\right)\frac{\epsilon^{2k}}{k!}\\ &\quad\times(\sin\varphi\sin\alpha\cos\beta+\cos\varphi\cos\alpha)^{2k}\\ &= 1-\frac{1}{2\sqrt{\pi}}\sum_{k=1}^{\infty}\Gamma\left(k-\frac{1}{2}\right)\frac{\epsilon^{2k}}{k!}\sum_{i=0}^{k}\binom{k}{i}\\ &\quad\times(\sin\varphi\sin\alpha\cos\beta)^{2i}(\cos\varphi\cos\alpha)^{2k-2i}.\end{aligned} \tag{B10}$$

Substituting this in integral I of (B8) and integrating over β in the first resulting term, we obtain

$$\begin{aligned}I &= 2\pi\int_0^{\pi} d\alpha\frac{\sin\alpha}{(1-\epsilon^2\cos^2\alpha)^2} - \frac{1}{2\sqrt{\pi}}\sum_{k=1}^{\infty}\Gamma\left(k-\frac{1}{2}\right)\\ &\quad\times\frac{\epsilon^{2k}}{k!}\sum_{i=0}^{k}\binom{k}{i}\sin^{2i}\varphi\cos^{2k-2i}\varphi\int_0^{2\pi} d\beta\cos^{2i}\beta\\ &\quad\times\int_0^{\pi} d\alpha\frac{\sin^{2i+1}\alpha\cos^{2k-2i}\alpha}{(1-\epsilon^2\cos^2\alpha)^2}.\end{aligned} \tag{B11}$$

The integration follows then with the aid of formulas 2.153 (3), 3.682, and 3.681 (1) of Ref. [44], obtaining with (B8) the

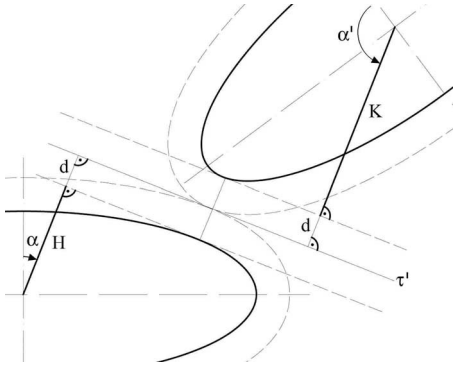

FIG. 8. Two oblate spheroids surrounded with shells of constant thickness which are in contact (2D representation).

expression for the *excluded volume of two identical oblate spheroids*:

$$V_{\mathrm{ex}}(\varphi) = 2V + 2a^3(1-\epsilon^2)\Bigg[4\pi F(2,1/2,3/2,\epsilon^2) - \sqrt{\pi}\sum_{k=1}^{\infty}\Gamma\left(k-\frac{1}{2}\right)\epsilon^{2k}\sum_{i=0}^{k}\frac{\sin^{2i}\varphi\cos^{2k-2i}\varphi}{2^i(k-i)!(i!)^2} \times B\left(i+1,\frac{2k-2i+1}{2}\right) \times F\left(2,\frac{2k-2i+1}{2},\frac{2k+3}{2},\epsilon^2\right)\Bigg]. \tag{B12}$$

Here, B is the beta function and F is the hypergeometric function. Let us now consider the situation depicted in Fig. 8 which represents two (identical) spheroids surrounded with a shell of constant thickness d. We are again interested in evaluating the excluded volume of these objects which, because of the constant shell offset, will no longer be ellipsoids. Nevertheless, we see that in this case we can again construct geometrical quantities like H and K of the two spheroids of Fig. 7 and that these, which we will call H' and K', are parallel to the old H and K, respectively. Then it follows that

$$H'(\alpha) = H(\alpha) + d, \tag{B13}$$

$$K'(\alpha') = K(\alpha') + d, \tag{B14}$$

and H and K will be given by (B1) and (B2). Now, in this case also expression (B5) holds true and, observing that the volume of an ovaloid may be written as [41,42]

$$V = \frac{1}{6}\int G(G,G)d\omega, \tag{B15}$$

where G is a geometric quantity constructed like H,K,H',K', we are able to write for the excluded volume of the two spheroids with shell

$$V_{\mathrm{exd}} = 2V' + \int K'(H',H')d\omega = V_{\mathrm{ex}} + \frac{4d}{3}\underbrace{\int (H,H)d\omega}_{I_1} + 2d\underbrace{\int\left(\frac{H}{3}+\frac{4d}{3}\right)\left(\frac{\partial^2 H}{\partial\alpha^2}+\frac{\cos\alpha}{\sin\alpha}\frac{\partial H}{\partial\alpha}+2H+d\right)d\omega}_{I_2} + 2d\underbrace{\int K\left(\frac{\partial^2 H}{\partial\alpha^2}+\frac{\cos\alpha}{\sin\alpha}\frac{\partial H}{\partial\alpha}+2H+d\right)d\omega}_{I_3}, \tag{B16}$$

and V_{ex} is the excluded volume of the two spheroids (B12).

Integrals I_1 and I_2 are straightforward and may be solved with the aid of formulas 3.682, 2.583 (3), 2.584 (3), and 2.584 (39) of [44]:

$$I_1 = 2a^2(1-\epsilon^2)\int_0^{2\pi}d\beta\int_0^{\pi}d\alpha\frac{\sin\alpha}{(1-\epsilon^2\cos^2\alpha)^2} = 8\pi a^2(1-\epsilon^2)F(2,1/2,3/2,\epsilon^2), \tag{B17}$$

$$I_2 = \int_0^{2\pi}d\beta\int_0^{\pi}d\alpha\sin\alpha\left(\frac{a\sqrt{1-\epsilon^2\cos^2\alpha}}{3}+\frac{4d}{3}\right) \times\left(\frac{a}{\sqrt{1-\epsilon^2\cos^2\alpha}}+\frac{a(1-\epsilon^2)}{(1-\epsilon^2\cos^2\alpha)^{3/2}}+d\right) = \frac{4\pi}{3}(a^2+4d^2)+6\pi ad\left(\sqrt{1-\epsilon^2}+\frac{\arcsin\epsilon}{\epsilon}\right) + \frac{4\pi}{3}a^2(1-\epsilon^2)\frac{\operatorname{arctanh}\epsilon}{\epsilon}. \tag{B18}$$

Regarding I_3 we have, using Eqs. (B2), (B4), and (B9),

$$I_3 = a\int_0^{2\pi}d\beta\int_0^{\pi}d\alpha\sin\alpha \times\sqrt{1-\epsilon^2(\sin\varphi\sin\alpha\cos\beta+\cos\varphi\cos\alpha)^2} \times\left(\frac{a}{\sqrt{1-\epsilon^2\cos^2\alpha}}+\frac{a(1-\epsilon^2)}{(1-\epsilon^2\cos^2\alpha)^{3/2}}+d\right), \tag{B19}$$

and we can again expand the $1-\epsilon^2(\sin\varphi\sin\alpha\cos\beta+\cos\varphi\cos\alpha)^2$ square root, obtaining

$$I_3 = a\int_0^{2\pi}d\beta\int_0^{\pi}d\alpha\sin\alpha\left(\frac{a}{\sqrt{1-\epsilon^2\cos^2\alpha}} + \frac{a(1-\epsilon^2)}{(1-\epsilon^2\cos^2\alpha)^{3/2}}+d\right) - \frac{a}{2\sqrt{\pi}} \times\sum_{k=1}^{\infty}\Gamma\left(k-\frac{1}{2}\right)\frac{\epsilon^{2k}}{k!}\sum_{i=0}^{k}\binom{k}{i}\sin^{2i}\varphi\cos^{2k-2i}\varphi \times\int_0^{2\pi}d\beta\cos^{2i}\beta\left(a\int_0^{\pi}d\alpha\frac{\sin^{2i+1}\alpha\cos^{2k-2i}\alpha}{\sqrt{1-\epsilon^2\cos^2\alpha}}\right.$$

$$+a(1-\epsilon^2)\int_0^{\pi} d\alpha \frac{\sin^{2i+1}\alpha \cos^{2k-2i}\alpha}{(1-\epsilon^2\cos^2\alpha)^{3/2}} + d\int_0^{\pi} d\alpha \sin^{2i+1}\alpha \cos^{2k-2i}\alpha\Bigg). \tag{B20}$$

These integrals may be solved again with the use of the formulas 2.153 (3), 3.682, 3.681 (1), 2.583 (3), 2.584 (39), and 3.621 (5) of [44], yielding

$$I_3 = 4\pi a\left(\frac{a\arcsin\epsilon}{\epsilon} + a\sqrt{1-\epsilon^2} + 2d\right) - a\sqrt{\pi}\sum_{k=1}^{\infty}\Gamma\left(k-\frac{1}{2}\right)\epsilon^{2k}\sum_{i=0}^{k}\frac{\sin^{2i}\varphi\cos^{2k-2i}\varphi}{2^i(k-i)!(i!)^2} \times B\left(i+1,\frac{2k-2i+1}{2}\right)\left[aF\left(\frac{1}{2},\frac{2k-2i+1}{2},\frac{2k+3}{2},\epsilon^2\right) + a(1-\epsilon^2)F\left(\frac{3}{2},\frac{2k-2i+1}{2},\frac{2k+3}{2},\epsilon^2\right) + d\right]. \tag{B21}$$

We can then combine all these results together with the property [45]

$$F\left(2,\frac{1}{2},\frac{3}{2},\epsilon^2\right) = \frac{1}{2}\left(\frac{1}{1-\epsilon^2} + \frac{\operatorname{arctanh}\epsilon}{\epsilon}\right) \tag{B22}$$

and Eq. (B16) to write the *excluded volume of two oblate spheroids surrounded by a shell of constant thickness* V_{exd}:

$$V_{\mathrm{exd}} = V_{\mathrm{ex}} + \frac{8\pi}{3}d(3a^2+4d^2+3ad) + 4\pi ad(2a+3d) \times\left(\sqrt{1-\epsilon^2} + \frac{\arcsin\epsilon}{\epsilon}\right) + 8\pi a^2 d(1-\epsilon^2)\frac{\operatorname{arctanh}\epsilon}{\epsilon} - 2ad\sqrt{\pi}\sum_{k=1}^{\infty}\Gamma\left(k-\frac{1}{2}\right)\epsilon^{2k}\sum_{i=0}^{k}\frac{\sin^{2i}\varphi\cos^{2k-2i}\varphi}{2^i(k-i)!(i!)^2} \times B\left(i+1,\frac{2k-2i+1}{2}\right)\left[aF\left(\frac{1}{2},\frac{2k-2i+1}{2},\frac{2k+3}{2},\epsilon^2\right) + a(1-\epsilon^2)F\left(\frac{3}{2},\frac{2k-2i+1}{2},\frac{2k+3}{2},\epsilon^2\right) + d\right]. \tag{B23}$$

We note that the above procedure allowed us to obtain an expression for V_{exd} with an angular dependence only upon φ. However, the orientation of the surface enclosing this volume will be dependent also on θ, which is why it is needed, e.g., in (6).

The above results can also be easily used to compute the *total volume of the spheroid with the shell* starting from Eq. (B15) with Eq. (B13):

$$V_d = V + \frac{d}{6}\int (H,H)d\omega + \frac{d}{3} \times \int (H+d)\left(\frac{\partial^2 H}{\partial\alpha^2} + \frac{\cos\alpha}{\sin\alpha}\frac{\partial H}{\partial\alpha} + 2H + d\right)d\omega, \tag{B24}$$

which is very similar to the first part of Eq. (B16) and can be integrated in the same way, obtaining

$$V_d = V + \frac{2\pi d}{3}\left[3a^2(1-\epsilon^2)\frac{\operatorname{arctanh}\epsilon}{\epsilon} + 3ad\left(\sqrt{1-\epsilon^2} + \frac{\arcsin\epsilon}{\epsilon}\right) + 3a^2 + 2d^2\right]. \tag{B25}$$

We now want to calculate the averaged excluded volume starting from the angle distribution functions which arise in the spheroid distributions of the simulation algorithm. For axially symmetric objects the angle distribution function $\Phi(\varphi)$ is dependent only on the angle between the symmetry axes, φ. In the case of an isotropic (or Poissonian) angle distribution, where any orientation is equally probable, it is easy to find

$$\Phi_{\mathrm{isotr}}(\varphi) = \frac{\sin\varphi}{4\pi}. \tag{B26}$$

To verify that this situation occurs without bias in the simulations, we used a modified version of the spheroid distribution creation algorithm: after the distribution was realized, for every spheroid it was searched for neighbors which lay within a certain radius from its center and the angles between their symmetry axis were recorded. We then fitted the function to the simulated angle distribution results and, although we may expect that this distribution function will deviate from the purely isotropic case when highly packed assemblies are realized due to local orientation, we obtained no deviation for all binning radii and all volume fractions considered in the present research. The averaged excluded volume of the two spheroids will then be

$$\langle V_{\mathrm{ex}}\rangle_{\mathrm{isotr}} = \int_0^{2\pi} d\theta\int_0^{\pi} d\varphi\Phi_{\mathrm{isotr}}(\varphi)V_{\mathrm{ex}}(\varphi) = \frac{1}{2}\int_0^{\pi} d\varphi\sin\varphi\, V_{\mathrm{ex}}(\varphi). \tag{B27}$$

This easily leads with (B12) and 3.621 (5) of [44] to the *averaged excluded volume of two oblate spheroids*:

$$\langle V_{\mathrm{ex}}\rangle = 2V + 8\pi a^3(1-\epsilon^2)F(2,1/2,3/2,\epsilon^2) - \sqrt{\pi}a^3(1-\epsilon^2) \times\sum_{k=1}^{\infty}\Gamma\left(k-\frac{1}{2}\right)\epsilon^{2k}\sum_{i=0}^{k}\frac{\left[B\left(i+1,\frac{2k-2i+1}{2}\right)\right]^2}{2^i(k-i)!(i!)^2} \times F\left(2,\frac{2k-2i+1}{2},\frac{2k+3}{2},\epsilon^2\right), \tag{B28}$$

and with Eq. (B23) and the same formula of [44] to the

averaged excluded volume of two oblate spheroids surrounded a shell of constant thickness:

$$\langle V_{\mathrm{exd}}\rangle = \langle V_{\mathrm{ex}}\rangle + \frac{8\pi}{3}d(3a^2+4d^2+3ad) + 4\pi ad(2a+3d) \times\left(\sqrt{1-\epsilon^2}+\frac{\arcsin\epsilon}{\epsilon}\right) + 8\pi a^2 d(1-\epsilon^2)\frac{\operatorname{arctanh}\epsilon}{\epsilon} - ad\sqrt{\pi}\sum_{k=1}^{\infty}\Gamma\left(k-\frac{1}{2}\right)\epsilon^{2k}\sum_{i=0}^{k}\frac{\left[B\left(i+1,\frac{2k-2i+1}{2}\right)\right]^2}{2^i(k-i)!(i!)^2} \times\left[aF\left(\frac{1}{2},\frac{2k-2i+1}{2},\frac{2k+3}{2},\epsilon^2\right)+a(1-\epsilon^2)F\left(\frac{3}{2},\frac{2k-2i+1}{2},\frac{2k+3}{2},\epsilon^2\right)+d\right]. \quad \text{(B29)}$$

The quantities involved in Eqs. (B28) and (B29) can then be easily evaluated with mathematical software like MAPLE [45].

The averaged excluded volume of the hard spheroids (B28) is of course equivalent to the Isihara-Ogston-Winzor expression [42,43]

$$\langle V_{\mathrm{ex}}\rangle_{\mathrm{IOW}} = \frac{4}{3}\pi a^2 b\left\{2+\frac{3}{2}\left(1+\frac{\arcsin\epsilon}{\epsilon\sqrt{1-\epsilon^2}}\right)\times\left[1+\frac{(1-\epsilon^2)}{2\epsilon}\ln\left(\frac{1+\epsilon}{1-\epsilon}\right)\right]\right\}. \quad \text{(B30)}$$

These expressions were then successfully verified through simulation by generating a great number of randomly placed spheroid couples with fixed reciprocal orientation and seeing how many times their shells overlapped. The ratio of overlaps to the total trial number is then equal to the ratio of the excluded volume to the volume of the simulation cell. As an example, we may consider the plot of such a comparison for $\langle V_{\mathrm{exd}}\rangle$ (B29) for the $d/a=0.1765$ and $a=0.5$ case, as shown in Fig. 9. Convergence tests on the series were also performed.

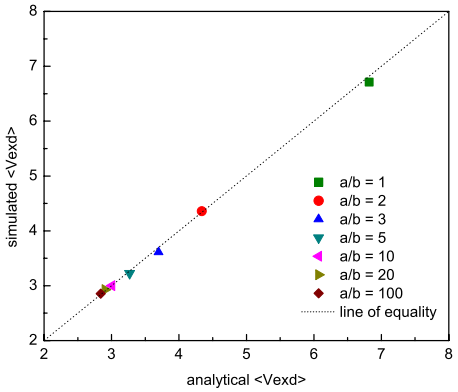

FIG. 9. (Color online) Comparison between the analytical and simulated values of $\langle V_{\mathrm{exd}}\rangle$ for the $d/a=0.1765$ and $a=0.5$ case and for different aspect ratios. Simulation data: $L/2a=40$, trial placing number$=10^7$.

It is finally interesting to observe that the ratio between $\langle V_{\mathrm{exd}}\rangle$ and the spheroid volume V is roughly linearly dependent upon the spheroid aspect ratio and that it slightly deviates from this behavior only close to the sphere case. The same holds true for the averaged excluded volume $\langle V_{\mathrm{ex}}\rangle$, showing that interpretion of the influence of the spheroid aspect ratio as an excluded volume effect is a consistent approach.

[1] D. M. Heyes, M. Cass, and A. C. Brańca, Mol. Phys. **104**, 3137 (2006).
[2] S. B. Lee and T. J. Yoon, J. Korean Phys. Soc. **33**, 612 (1998).
[3] S. F. Wang and A. A. Ogale, Compos. Sci. Technol. **46**, 93 (1993).
[4] I. Balberg and N. Binenbaum, Phys. Rev. A **35**, 5174 (1987).
[5] V. K. S. Shante and S. Kirkpatrik, Adv. Phys. **20**, 325 (1971).
[6] H. Scher and R. Zallen, J. Chem. Phys. **53**, 3759 (1970).
[7] Z. Néda, R. Florian, and Y. Brechet, Phys. Rev. E **59**, 3717 (1999).
[8] A. L. R. Bug, S. A. Safran, and I. Webman, Phys. Rev. Lett. **54**, 1412 (1985).
[9] A. L. R. Bug, S. A. Safran, and I. Webman, Phys. Rev. B **33**, 4716 (1986).
[10] I. Balberg, N. Binenbaum, and N. Wagner, Phys. Rev. Lett. **52**, 1465 (1984).
[11] I. Balberg, C. H. Anderson, S. Alexander, and N. Wagner, Phys. Rev. B **30**, 3933 (1984).
[12] L. Berhan and A. M. Sastry, Phys. Rev. E **75**, 041121 (2007).
[13] A. Celzard, E. McRae, C. Deleuze, M. Dufort, G. Furdin, and J. F. Marêché, Phys. Rev. B **53**, 6209 (1996).
[14] E. Charlaix, J. Phys. A **19**, L533 (1986).
[15] E. Charlaix, E. Guyon, and N. Rivier, Solid State Commun. **50**, 999 (1984).
[16] Y. B. Yi, C. W. Wang, and A. M. Sastry, J. Electrochem. Soc. **151**, A1292 (2004).
[17] Y. B. Yi and A. M. Sastry, Proc. R. Soc. London, Ser. A **460**, 2353 (2004).
[18] E. J. Garboczi, K. A. Snyder, J. F. Douglas, and M. F. Thorpe, Phys. Rev. E **52**, 819 (1995).
[19] E. M. Sevick, P. A. Monson, and J. M. Ottino, Phys. Rev. A **38**, 5376 (1988).
[20] A. S. Skal and B. I. Shklovskii, Sov. Phys. Semicond. **7**, 1058 (1974).
[21] T. Schilling, S. Jungblut, and M. A. Miller, Phys. Rev. Lett. **98**, 108303 (2007).
[22] L. Berhan and A. M. Sastry, Phys. Rev. E **75**, 041120 (2007).
[23] A. A. Ogale and S. F. Wang, Compos. Sci. Technol. **46**, 379 (1993).
[24] D. P. Bentz, J. T. G. Hwang, C. Hagwood, E. J. Garboczi, K. A. Snyder, N. Buenfeld, and K. L. Scrivener, in *Microstructure of Coment-Based Systems/Bonding and Interfaces in Comenti-*

tious Materials, edited by S. Diamond, F. P. Glasser, L. D. Wakely, S. Mindess, J. Skalny, and L. Roberts, MRS Symposia Proceedings No. 370 (Materials Research Society, Pittsburgh, 1995), p. 437.
[25] S. Akagawa and T. Odagaki, Phys. Rev. E **76**, 051402 (2007).
[26] A. Donev, S. Torquato, and F. H. Stillinger, J. Comput. Phys. **202**, 765 (2005).
[27] J. W. Perram and M. S. Wertheim, J. Comput. Phys. **58**, 409 (1985).
[28] J. Vieillard-Baron, J. Chem. Phys. **56**, 4729 (1972).
[29] E. Rimon and S. P. Boyd, J. Intell. Robotic Syst. **18**, 105 (1997).
[30] E. Rimon and S. P. Boyd, Stanford University ISL Technical report, 1992 (unpublished).
[31] N. Johner, C. Grimaldi, I. Balberg, and P. Ryser, Phys. Rev. B **77**, 174204 (2008).
[32] A. Al-Futaisi and T. W. Patzek, Physica A **321**, 665 (2003).
[33] J. Hoshen and R. Kopelman, Phys. Rev. B **14**, 3438 (1976).
[34] J. D. Sherwood, J. Phys. A **30**, L893 (1997).
[35] M. D. Rintoul and S. Torquato, J. Phys. A **30**, L585 (1997).
[36] This may be illustrated more concretely by considering one specific example: for aspect ratio $a/b=3$ and shell thickness $d/a=0.1111$, 30 realizations per cell size led to a percolation threshold for the infinite system of $\phi_c=0.2612\pm0.0008$, while 100 realizations led to $\phi_c=0.2613\pm0.0003$ and 200 realizations led to $\phi_c=0.26125\pm0.00025$. It can be seen that, even with 30 realizations the error bar was only $\pm0.4\%$ and that 100 realizations, as used for all the $d/a=0.1111$ cases, did not lead to significantly less precision when compared to 200 realizations.
[37] W. Lu, J. Weng, D. Wu, C. Wu, and G. Chen, Mater. Manuf. Processes **21**, 167 (2006).
[38] G. Chen, C. Wu, W. Weng, D. Wu, and W. Yan, Polymer **44**, 1781 (2003).
[39] S. Stankovich, D. A. Dikin, G. H. B. Dommett, K. M. Kohlhaas, E. J. Zimney, E. A. Stach, R. D. Piner, S. T. Nguyen, and R. S. Ruoff, Nature (London) **442**, 282 (2006).
[40] A. Trokhymchuk, I. Nezbeda, J. Jirsák, and D. Henderson, J. Chem. Phys. **123**, 024501 (2005).
[41] A. Isihara, J. Chem. Phys. **19**, 1142 (1951).
[42] A. Isihara, J. Chem. Phys. **18**, 1446 (1950).
[43] A. G. Ogston and D. J. Winzor, J. Phys. Chem. **79**, 2496 (1975).
[44] I. S. Gradshteyn and I. M. Ryzhik, *Table of Integrals, Series, and Products* (Academic Press, San Diego, 2000).
[45] Computer code MAPLE (Waterloo Maple, Waterloo, 2006).